Scattering from Several Test-Objects Computed by 3-D Hybrid IE/PDE Methods

Paul Soudais, *Member, IEEE*, Hervé Stève, and Fabrice Dubois

***Abstract*—The electromagnetic scattering from composite anisotropic dielectric and conducting structures is modeled by hybrid partial differential equation—integral equation formulations. We emphasize the role of edge elements for both the partial differential equation and the integral equation discretization and for the coupling of the two. Numerical results from the various formulations presented here and measurements are compared in order to obtain test cases for the development and validation of numerical methods.**

***Index Terms*—Electromagnetic scattering, FEM, integral equations, Method of Moments, partial differential equations.**

I. Introduction

RECENTLY, partial differential equation and integral equation solution methods have been combined into general purpose formulations for scattering computations. The partial differential equations are well suited for the modeling of inhomogeneous anisotropic scatterers. Whereas integral equations can be used to model homogeneous regions and are also particularly useful to model the unbounded free-space problem. The integral equation can thus provide an exact boundary condition for the partial differential equations.

The finite element discretization of the partial differential equations arising from time-harmonic Maxwell equations is often based on so-called H(curl) "edge" elements [1]–[5]. These elements are free of spurious modes and lead to the correct field continuity properties at the interface between different media.

Secondly, integral equations are mostly discretized with H(div) "edge" boundary elements [6]–[9] which are free of line and point charges.

Several authors [2], [10]–[13] have presented hybrid formulations discretized with the finite element/boundary element method. Some authors combined H(div) and H(curl) elements for the discretization [14]–[17]. We emphasize in this report the relationship between the two families of edge elements which makes this hybrid discretization possible.

Since we have two partial differential equations and two integral equations, a number of different hybrid formulations can be constructed. We shall compare some of them with different discretizations (linear P1 elements, $\mathbf{J}$ and $\mathbf{E}$ with Hdiv elements, $\mathbf{J}$ and $\mathbf{K}$ with Hdiv elements).

Manuscript received December 29, 1997; revised August 20, 1998.

P. Soudais is with ONERA, BP 7292322, Chatillon Cedex, France.

H. Stève and F. Dubois are with Dassault-Aviation, 92214 Saint-Cloud, France.

Publisher Item Identifier S 0018-926X(99)04770-5.

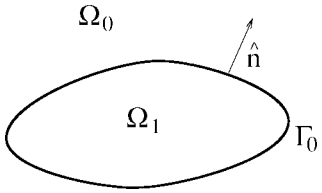

Fig. 1. Scatterer and exterior medium.

In this article, we continue a work that has been initiated in the 1990, 1992, and 1994 JINA RCS Workshops, in order to obtain reference solutions that can be used for code development and validation. We present solutions for an anisotropic sphere with lossy and symmetric electromagnetic properties and also with unlossy antisymmetric properties. A number of computed solutions of the scattering by a perfectly electrically conducting (PEC) plate, coated with inhomogeneous dielectric, are compared to measurements. Finally, computations on an inhomogeneous prismatic cylinder made of three different materials (PEC, isotropic dielectric, anisotropic dielectric) are compared.

II. Formulation

Consider a scatterer of volume Ω_1 surrounded by a homogeneous medium Ω_0. The surrounding medium has permittivity ε_0 and permeability μ_0. The scatterer is illuminated by an incident wave $\{\mathbf{E}_i, \mathbf{H}_i\}$ with wavenumber k.

The weak form of the partial differential equation for the interior problem in Ω_1 relates the electric field $\mathbf{E}$ in the volume to the trace of the tangential magnetic field (or equivalently $n \times \mathbf{H}$) on its boundary Σ_0,

$$j \int_{\Omega_1} k^2(\varepsilon \mathbf{E}) \cdot \mathbf{\Phi}\, dv - (\mu^{-1} \nabla \times \mathbf{E}) \cdot (\nabla \times \mathbf{\Phi})\, dv - k \int_{\Sigma_0} \mathbf{\Phi} \cdot (\hat{n} \times \mathbf{H})\, ds = 0. \quad (1)$$

The scatterer can be made of inhomogeneous dielectric, in this case the complex permittivity and permeability (ε_n, μ_n) are complex valued functions of the position (complex (3×3) matrices for anisotropic materials).

Alternatively, a weak equation can be derived relating $\mathbf{H}$ in Ω_1 to $\hat{n} \times \mathbf{E}$ on its boundary

$$j \int_{\Omega_1} k^2(\mu \mathbf{H}) \cdot \mathbf{\Phi}\, dv - (\varepsilon^{-1} \nabla \times \mathbf{H}) \cdot (\nabla \times \mathbf{\Phi})\, dv + k \int_{\Sigma_0} \mathbf{\Phi} \cdot (\hat{n} \times \mathbf{E})\, ds = 0. \quad (2)$$

The exterior problem (in the unbounded region Ω_0) is recast on the surface Σ_0 by means of an integral equation. We can use either the electric field integral equation (EFIE) or the magnetic field integral equation (MFIE). The EFIE and MFIE, written in weak form, are given by

$$\frac{j}{4\pi}\iint_{\Sigma_0}\{k^2G(\mathbf{\Phi}\cdot\mathbf{J}')-G((\nabla_S\cdot\mathbf{\Phi})(\nabla'_S\cdot\mathbf{J}'))\}\,ds\,ds' + \frac{k}{2}\int_{\Sigma_0}\mathbf{\Phi}\cdot(\hat{n}\times\mathbf{K})\,ds+\frac{k}{4\pi}\iint_{\Sigma_0\setminus M}(\nabla' G) \cdot(\mathbf{\Phi}\times\mathbf{K}')\,ds\,ds' = k\int_{\Sigma_0}\mathbf{\Phi}\cdot\mathbf{E}_i\,ds \tag{3}$$

$$-\frac{k}{2}\int_{\Sigma_0}\mathbf{\Phi}\cdot(\hat{n}\times\mathbf{J})\,ds-\frac{k}{4\pi}\iint_{\Sigma_0\setminus M}(\nabla' G)\cdot(\mathbf{\Phi}\times\mathbf{J}')\,ds\,ds' + \frac{j}{4\pi}\iint_{\Sigma_0}\{k^2G(\mathbf{\Phi}\cdot\mathbf{K}')-G((\nabla_S\cdot\mathbf{\Phi})(\nabla'_S\cdot\mathbf{K}'))\}\,ds\,ds' = k\int_{\Sigma_0}\mathbf{\Phi}\cdot\mathbf{H}_i\,ds \tag{4}$$

with $\mathbf{J}=\hat{n}\times\mathbf{H}$, $\mathbf{K}=\mathbf{E}\times\hat{n}$, $G(r)=e^{-jkr}/r$, $r=\|\overrightarrow{MM'}\|$, $k=\omega/c$, the primed quantities (e.g., $\mathbf{J}'$) are taken at the emission point M', the others are taken at the observation point M.

The interior problem (1) or (2) is discretized with tetrahedral curl-conforming edge elements [1]. These elements guarantee that the null-space of the curl operator is correctly approximated (no spurious modes are added to the solution). With these elements, only the tangential components of the field are continuous at element boundaries, i.e., the normal components are allowed to jump which is the correct physical property.

The boundary problem is discretized with triangular divergence-conforming basis functions $\mathbf{f}_i$ [6], which have become very popular since the classical article [7].

The trace of the volume basis function $\mathbf{w}_i$ on a triangle is related to the corresponding surface Rao–Wilton–Glisson basis function by

$$-\hat{n}\times\mathbf{w}_i=\mathbf{f}_i$$

(see Appendix A). If $\mathbf{E}$ is discretized with volume H(curl) elements, the trace of $\mathbf{E}$ on the surface **is** indeed a magnetic current $\mathbf{K}$ discretized with H(div) elements. The same correspondance holds for $\mathbf{H}$ and $-\mathbf{J}$, and for the test-functions.

The boundary condition on conducting surfaces is enforced by setting $\hat{n}\times\mathbf{E}$ (or, equivalently, the tangential part of $\mathbf{E}$) to zero and thus removing the corresponding unknowns.

So the unknowns of the problem are

$$\begin{aligned}\mathbf{J}=\hat{n}\times\mathbf{H} &\quad \text{on } \Sigma_0\\ \mathbf{K}_d=\mathbf{E}_d\times\hat{n} &\quad \text{on } \Sigma_d, \text{the nonconducting part of } \Sigma_0\\ \mathbf{E}_{\text{int}} &\quad \text{on nonconducting edges internal to } \Omega_1\\ \text{or } \mathbf{H}_{\text{int}} &\quad \text{on edges internal to } \Omega_1.\end{aligned}$$

Several formulations of the scattering problem can be based on (1)–(4). Below we shall discuss two symmetric formulations and two nonsymmetric formulations. It is noteworthy that symmetric formulations do not need more assembly operations or storage than the nonsymmetric ones, since only half of the coefficient needs to be calculated. Moreover, a dedicated symmetric solver can be used to speed up the solution and a symmetric operator is expected to be more robust. However, nonsymmetric formulations can advantageously be solved in two steps: a sparse matrix solution and dense matrix solution.

1) Symmetric Formulations A symmetric formulation can be obtained by selecting (1) and (3), adding the redundant equation (4) to (1) and using $j\mathbf{K}$ and $j\mathbf{E}$ as unknowns rather than $\mathbf{K}$ and $\mathbf{E}$

$$\begin{bmatrix} B_{00}-S_{00} & P_{0d}+Q_{0d} & 0\\ {}^tP_{0d}+Q_{d0} & B_{dd}-S_{dd}+M_{dd} & M_{d,\text{int}}\\ 0 & {}^tM_{d,\text{int}} & M_{\text{int,int}}\end{bmatrix}\begin{bmatrix}\mathbf{J}\\ j\mathbf{K}_d\\ j\mathbf{E}_{\text{int}}\end{bmatrix} = \begin{bmatrix}2P_{00}(j\mathbf{E}_{i,0}\times\hat{n})\\ 2P_{dd}(\hat{n}\times\mathbf{H}_{i,d})\\ 0\end{bmatrix} \tag{5}$$

with

$$\begin{aligned}\langle(B-S)\mathbf{A}',\mathbf{\Phi}\rangle &= \frac{j}{4\pi}\iint_{\Sigma_0}\{k^2G(\mathbf{\Phi}\cdot\mathbf{A}') - G((\nabla_S\cdot\mathbf{\Phi})(\nabla'_S\cdot\mathbf{A}'))\}\,ds\,ds'\\ \langle Q\mathbf{A}',\mathbf{\Phi}\rangle &= -\frac{jk}{4\pi}\iint_{\Sigma_0\setminus M}(\nabla' G)\cdot(\mathbf{\Phi}\times\mathbf{A}')\,ds\,ds'\\ \langle P\mathbf{A},\mathbf{\Phi}\rangle &= -\frac{jk}{2}\int_{\Sigma_0}\mathbf{\Phi}\cdot(\hat{n}\times\mathbf{A})\,ds\\ \langle M\mathbf{E},\mathbf{\Psi}\rangle &= jk^2\int_{\Omega_d}(\varepsilon\mathbf{E})\cdot\mathbf{\Psi}\,dv - j\int_{\Omega_d}(\mu^{-1}\nabla\times\mathbf{E})\cdot(\nabla\times\mathbf{\Psi})\,dv.\end{aligned}$$

The indexes (e.g., $0d$) in the $\langle Q_{0d}\mathbf{A}',\mathbf{\Phi}\rangle$ notation indicate the surfaces on which the integration is carried out

$$\langle Q_{0d}\mathbf{A}'_d,\mathbf{\Phi}\rangle=-\frac{jk}{4\pi}\int_{\Sigma_d}\left\{\int_{\Sigma_0\setminus M}(\nabla' G)\cdot(\mathbf{\Phi}\times\mathbf{A}'_d)\,ds\right\}ds'.$$

Operators $B-S$ and Q are complex symmetric, P is antisymmetric, M is symmetric if ε and μ are symmetric tensors. Note, that for a PEC scatterer this formulation yields the EFIE equation.

A dual symmetric formulation can be obtained by selecting (3) and the sum of (2) and (4)

$$\begin{bmatrix} B_{dd}-S_{dd} & P_{d0}+Q_{d0} & 0\\ {}^tP_{d0}+Q_{0d} & B_{00}-S_{00}+M'_{dd} & M'_{d,\text{int}}\\ 0 & {}^tM'_{d,\text{int}} & M'_{\text{int,int}}\end{bmatrix}\begin{bmatrix}j\mathbf{K}_d\\ \mathbf{J}\\ -\mathbf{H}_{\text{int}}\end{bmatrix} = \begin{bmatrix}2P_{dd}(\hat{n}\times\mathbf{H}_{i,d})\\ 2P_{00}(\mathbf{E}_{i,0}\times\hat{n})\\ 0\end{bmatrix}. \tag{6}$$

A detailed analysis of these formulations, of the properties of the operators, proofs of the existence of a unique solution for the variational problem and for the discretized problem can be found in [16].

For test purposes we note that interchanging ε and μ, $\mathbf{E}_i$ and $\mathbf{H}_i$ in system (5) leads to (6) (the unknowns $\mathbf{J}, j\mathbf{K}, j\mathbf{E}$ are changed to $j\mathbf{K}, \mathbf{J}, -\mathbf{H}$ in the process). This allows us to test the two formulations with the same code (as long as there are no PEC conditions).

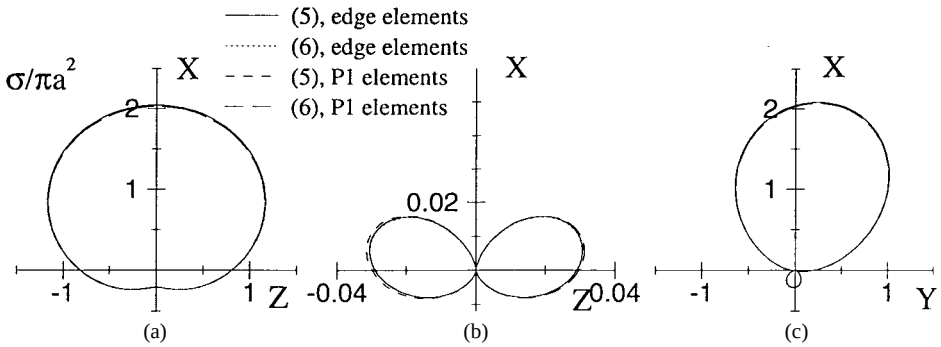

Fig. 2. Bistatic RCS of an anisotropic sphere with material characteristics (7). (a) copolarized RCS in the (Z, X) plane. (b) Cross-polarized RCS (Y component) in the (Z, X) plane, and (c) RCS in the (Y, X) plane.

The results presented hereafter for symmetric formulations have been obtained with the HEM3D code which implements formulation (5) discretized with edge elements. The hydrid dense/sparse linear system is solved with an iterative algorithm [5], which is efficient for hybrid dense/sparse systems with multiple right-hand sides. The HEM3D code runs on parallel machines or plain workstations. For dense systems it can also use a parallel out-of-core solver (which has mainly been Intel's DES-solver on Paragon so far).

B. Nonsymmetric Formulations

Selecting one partial differential equation [e.g., (1)] with one integral equation [e.g., (3)] leads to a coupled system of equations which can be solved in two steps [19], [20]. For instance solve first for $\mathbf{E}$ in terms of $\mathbf{J}$ from (1) (sparse matrix solution), replace $\mathbf{K}$ by $\hat{n} \times \mathbf{E}$ in (3) and solve for $\mathbf{J}$ (dense matrix solution). Then, specific optimized solvers can be used for each of the linear systems (e.g., sparse solver and dense out-of-core parallel solver).

Note, that the operators P and $P+Q$ are not invertible in the space H(div) (see Appendix B), therefore solving (3) for $\mathbf{K}$, would lead to very poor results. For this reason, we constructed the formulations with the operator $P+Q$ in off-diagonal blocks.

This difficulty with $P+Q$ has lead some authors [21] to discretize the integral equations with both $\mathbf{J}$ and $\mathbf{E}$ in the space H(div). In this case the operator $P+Q$ is replaced by an invertible operator. However, this strategy leads to unwanted field continuity at dielectric interfaces (continuity of normal component of $\mathbf{E}$ instead of continuity of the tangential component). We will present results using this strategy and, indeed, observe a strange behavior of the solution at the interfaces.

III. Test-Cases

A. Anisotropic Sphere

First we study the bistatic RCS of an anisotropic sphere at $ka = 1.125$ whose characteristics are

$$\varepsilon_r = \begin{pmatrix} 1.5-0.1j & 0 & 0 \\ 0 & 2.5-0.1j & 0 \\ 0 & 0 & 1.2-0.2j \end{pmatrix}$$
$$\mu_r = \begin{pmatrix} 2.5-1.8j & -0.5+0.5j & 0 \\ -0.5+0.5j & 2.5-1.8j & 0 \\ 0 & 0 & 1 \end{pmatrix}. \quad (7)$$

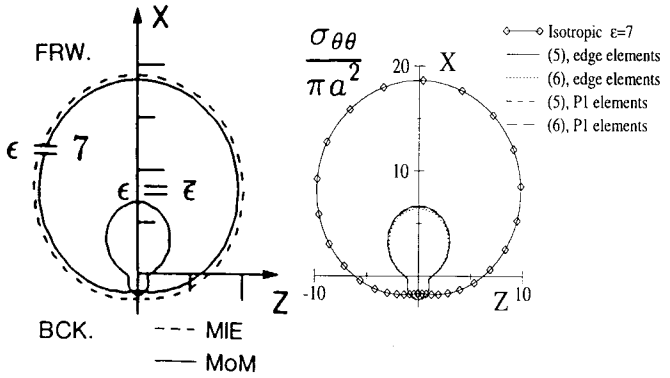

Fig. 3. Comparison of the RCS of an isotropic sphere ($\varepsilon = 7, \mu = 1$) with an anisotropic sphere with characteristics (8). The copolarized RCS in the (Z, X) plane of [22] is compared to the results of formulation (5) and (6) discretized with edge or P1 elements.

The wave vector $\vec{k}$ is directed along $\vec{x}$, the electric field $\mathbf{E}$ is directed along $\vec{z}$. The mesh leads to 1710 surface and 3061 volume unknowns.

In Fig. 2, we plot (a) the copolarized component in the $(\vec{x}, \vec{z})$ plane, (b) the cross-polarized component ($\vec{y}$ component in the $(\vec{x}, \vec{z})$ plane, and (c) the bistatic RCS in the $(\vec{x}, \vec{y})$ plane. We compare formulation (5) and (6), discretized with edge elements, and formulation (5) and (6), discretized with P1 elements [12], [13]. The anisotropic material gives rise to a cross-polarization. In addition, in the $(\vec{x}, \vec{y})$ plane the pattern is tilted due to the anisotropic material.

The four results are quasiidentical despite (a) the different discretizations (b) the different formulations. In the P1 discretization, $\nabla \cdot (\varepsilon \mathbf{E}) = 0$ is enforced via a projection method for formulation (5), similarly $\nabla \cdot (\mu \mathbf{H}) = 0$ is enforced for (6).

We proceed to test a configuration with an antisymmetric constitutive tensor without losses, the characteristics of the sphere are changed to

$$\varepsilon_r' = \begin{pmatrix} 7 & 0 & 0 \\ 0 & 7 & -3j \\ 0 & 3j & 7 \end{pmatrix}, \quad \mu_r = 1. \quad (8)$$

This corresponds to a case that has been presented in [22], where the computation was done with a method of moments for a volume integral equation. The copolarized bistatic radar cross section (RCS or σ) in the plane of incidence $(\vec{k}, \mathbf{E})$ is displayed in Fig. 3. The wave vector, incidence and ka remain the same as in the first case. The RCS in the shadow region is much lower in the anisotropic case than in the isotropic case.

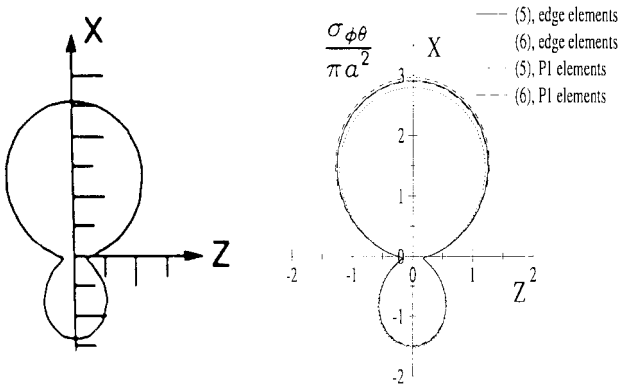

Fig. 4. Cross-polarized RCS in the (Z, X) plane of an anisotropic sphere with characteristics (8). The results of [22] are compared to the results of formulation (5) and (6) discretized with edge or P1 elements.

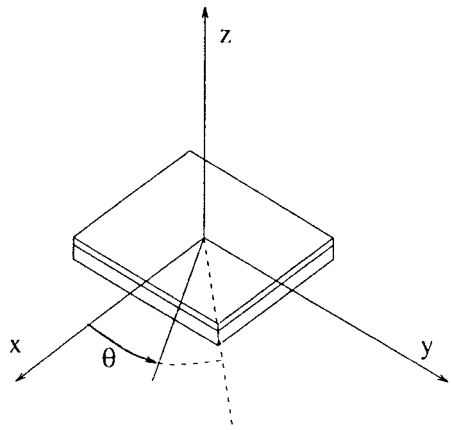

Fig. 5. Conducting plate coated on one side.

As a result, the component of the RCS in the $\vec{y}$ direction (cross-polarized), which is zero in the isotropic case, is of the order of magnitude of the copolarized RCS (Fig. 4). We compare here the numerical results of [22] (anisotropic volume method of moments) with the result of formulation (5) and (6) discretized with edge elements or P1 elements. The results obtained are very similar. We do see a little difference between formulation (5) and formulation (6) in the case of an antisymmetric unlossy material.

B. Conducting Plate Coated on One Side

We shall now study the monostatic RCS of a coated PEC plate with grazing incidence (Fig. 5). The grazing incidence makes it a difficult test-case with low-RCS (the RCS for normal incidence on the PEC plate is about 4 dB whereas the average RCS in ϕ polarization has a mean value of roughly -40 dB from 10° to 45°). Also the scattering from edges, corners and the junction between PEC and dielectric material must be modeled accurately.

The object is a square metallic plate of size $0.2 \times 0.2 \times 0.01$ m. One face is coated with 3 mm of dielectric material with $\varepsilon_r = 3.15 - 0.11j$, $\mu_r = 1$. The frequency is 3.2 GHz.

There are 9175 surface unknowns and 15 079 volume unknowns.

In Figs. 6 and 7 we compare measurements made at ONERA and three computational results. The IE/IE computation uses an integral formulation both for the interior and the exterior problem ($\mathbf{E}$ and $\mathbf{J}$ are discretized with H(div) elements). The IE/PDE edge result uses formulation (5) discretized with surface and volume elements. The IE/PDE P1 result corresponds to formulation (6) discretized with P1 elements (see [13]).

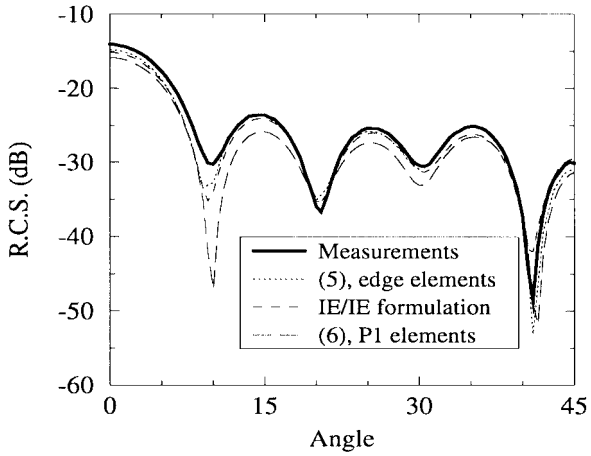

Fig. 6. Comparison of measured and computed RCS of a conducting plate $0.2 \times 0.2 \times 0.01$ m coated on one side with a dielectric. Grazing incidence, 3.2 GHz, $\theta\theta$ polarization.

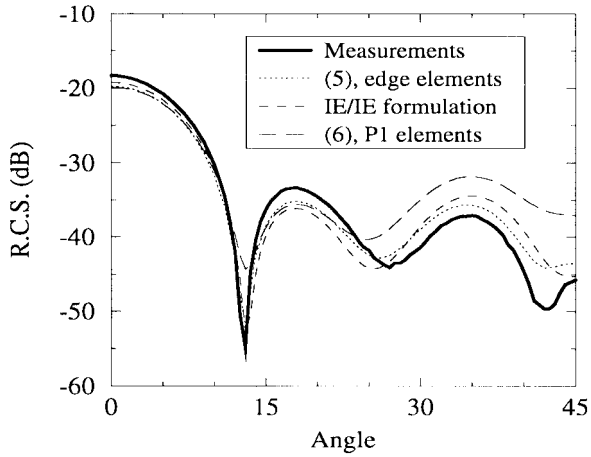

Fig. 7. Comparison of measured and computed RCS of a conducting plate $0.2 \times 0.2 \times 0.01$ m coated on one side with a dielectric. Grazing incidence, 3.2 GHz, $\phi\phi$ polarization.

The two numerical methods discretized with edge elements (IE/IE and IE/PDE) lead to similar results which are in agreement with the measurements. Significant differences appear with the P1 discretization mostly in the θ polarization where the scattering by the corners is important. We see that the edge elements discretization leads to good results for this low signature object with important corner diffraction.

C. Anisotropic/Isotropic/Conducting Prism

The next object we shall study, is a cylinder of finite height h composed of three different materials. A cross-sectional view of the prismatic cylinder is shown in Fig. 8. The cylinder axis is along $\vec{z}$, its cross section is in the $(\vec{x}, \vec{y})$ plane. The cross section of the cylinder is an isosceles triangle whose

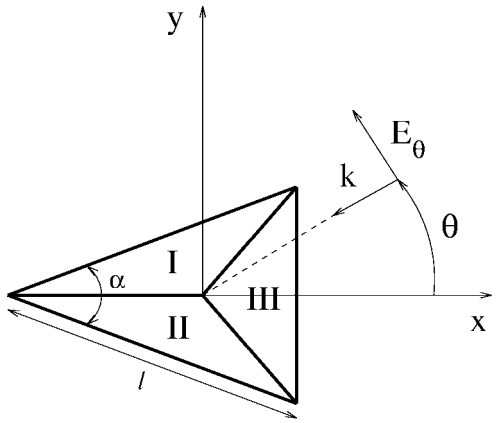

Fig. 8. Section view of the prism, θ polarization.

TABLE I
UNKNOWN COUNT FOR THE THREE MESHES OF THE PRISM

	mesh 1		mesh 2	mesh 3
	P1	Edges	Edges	Edges
Surfacic unknowns	3348	3239	7450	6860
Interior unknowns	3390	3680	12838	27765

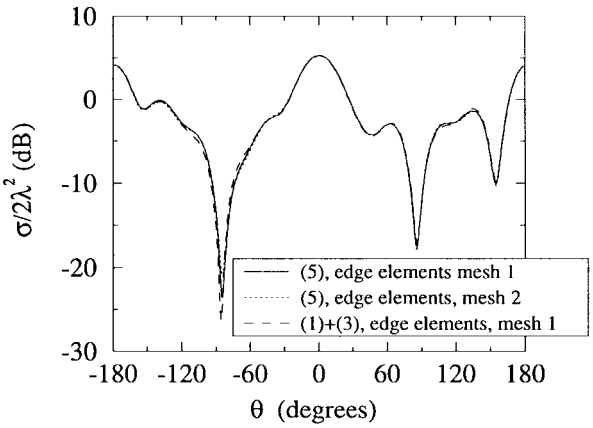

Fig. 9. RCS versus incidence angle of a prism made of three materials (PEC/isotropic/anisotropic), θ polarization.

medians divide it into three domains of different material characteristics. The first domain is a dielectric with relative permittivity and permeability $\varepsilon_{1r} = 1.4 - 0.7j$ and $\mu_{1r} = 1$, respectively. The characteristics of the second dielectric domain are

$$\varepsilon_{2r} = \begin{pmatrix} 2-0.1j & 0 & 0 \\ 0 & 2-0.1j & 0 \\ 0 & 0 & 1.2-0.2j \end{pmatrix}$$

$$\mu_{2r} = \begin{pmatrix} 2.5-1.8j & -0.5+0.5j & 0 \\ -0.5+0.5j & 2.5-1.8j & 0 \\ 0 & 0 & 1 \end{pmatrix}.$$

The third domain is perfectly conducting. The dimensions are related to the wavelength by $a = h = \lambda$ and $\alpha = 40°$. Figs. 9–12 show the RCS of this object versus the angle of incidence for incident waves with propagation direction in the $(\vec{x}, \vec{y})$ plane.

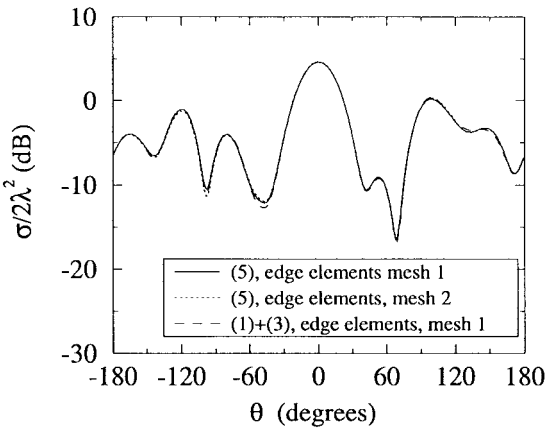

Fig. 10. RCS versus incidence angle of a prism made of three materials (PEC/isotropic/anisotropic), ϕ polarization.

Three different meshes of increasing density have been used.

We plot normalized monostatic diagrams $(\sigma/2\lambda^2)$ for polarizations θ and ϕ for $\theta = -180°$ to $\theta = 180°$. If the two dielectric materials were identical, we would have symmetric results, i.e., $\sigma(\theta) = \sigma(-\theta)$. The fact that the results are far from symmetric shows that this test-case is significant for the inhomogeneous dielectric object case.

The solutions from formulation (5) and the coupling of (1) and (3) discretized with edge elements compare very well (Fig. 9 and 10). Both formulations use H(div) elements for $\mathbf{J}$ and $\mathbf{K}$ discretization, H(curl) elements for $\mathbf{E}$. The coupled system (5) is solved in one step. Whereas (1) is solved for $\mathbf{E}$ in terms of $\mathbf{J}$ (sparse system solution), (3) is solved for $\mathbf{J}$ in terms of $\mathbf{K}$ on the PEC part of the outer surface, finally the system coupling $\mathbf{J}$ and $\mathbf{K}$ on the dielectric part of the boundary is solved. There is no significant difference in using the finer mesh (mesh 2). We consider one of these solutions (e.g., (5) with mesh 1) as our reference solution.

We proceed to compare the reference solution with other ones (Figs. 11 and 12). We note some differences between the reference solution and the coupling of (2) and (3) when both $\mathbf{J}$ and $\mathbf{E}$ are discretized with H(div) elements. We have also observed spurious components in $\mathbf{E}$ at material discontinuities when plotting $\mathbf{E}$ on the surface. The main differences in the RCS appear for θ polarization around $\theta = 0°$, when the incident electric field is normal to the dielectric/dielectric interface. The discretization of (6) with P1 elements also yields poorer results. This was expected and it confirms that this test-case is stringent.

IV. CONCLUSION

In this paper, we have presented several formulations of electromagnetic scattering problems and tested several discretizations in order to compare them with respect to accuracy. We have seen that a P1 finite element discretization with divergence constraints yields very good results, as long as the scatterer is entirely dielectric. The results were less good when part of the scatterer's outer surface was conducting. We have also seen that the discretization of both $\mathbf{E}$ and $\mathbf{J}$ with H(div)

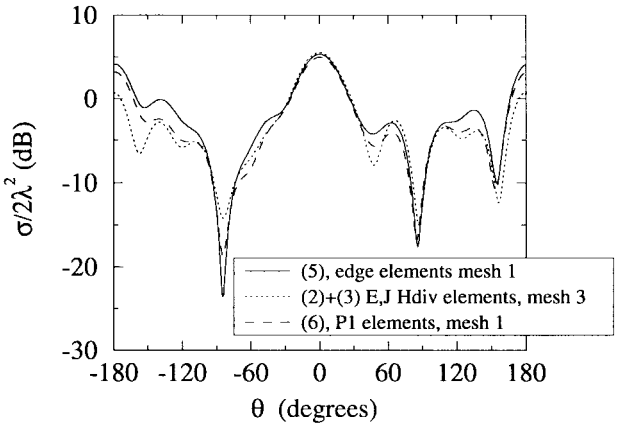

Fig. 11. Comparison of the RCS computed for the prism with different elements (P1 and different edge discretizations), θ polarization.

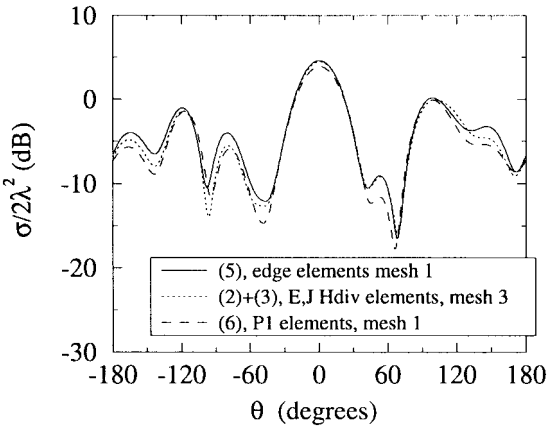

Fig. 12. Comparison of the RCS computed for the prism with different elements (P1 and different edge discretizations), ϕ polarization.

elements leads to improper modeling of dielectric interfaces and yielded not very accurate results on multidielectric objects.

We have stressed the fact that H(curl) volume elements are compatible with H(div) surface elements. In addition, the discretization of $\mathbf{E}$ or $\mathbf{H}$ with H(curl) elements and of $\mathbf{J}$ and $\mathbf{K}$ with H(div) elements leads to correct continuity conditions on dielectric/dielectric interfaces, PEC/dielectric interfaces and on the boundary of open PEC surfaces. Consequently, hybrid IE-PDE formulation with edge element discretization leads to a powerful general-purpose method.

Several test-cases have emerged with reference solutions and an idea of the accuracy that should be obtained. We will be glad to provide the meshes that we have used.

Appendix A
Triangle and Tetrahedral Edge Elements

For the discretization process we expand the fields on the basis functions

$$\hat{n}\times\mathbf{H}=\sum_{i=1}^{n}h_i\mathbf{f}_i$$
$$\mathbf{E}=\sum_{i=1}^{m}e_i\mathbf{w}_i$$

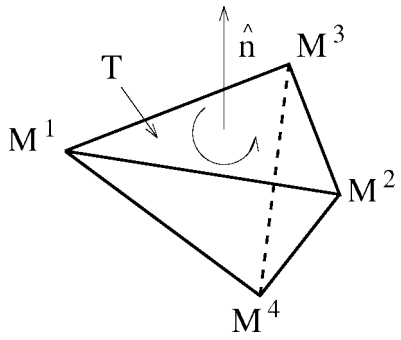

Fig. 13. (M^1, M^2, M^3, M^4) tetrahedral element and (M^1, M^2, M^3) triangle element.

the $\mathbf{f}_i$ being the surface edge element basis functions on triangles [7], [6] [or H(div)], and the $\mathbf{w}_i$ being the volume edge element basis fuctions on tetrahedrons [1]–[3] [or H(curl)]. We need to obtain $\mathbf{E}\times\hat{n}$ on the boundary of the scatterer.

The basis function associated with the edge 2–3 of the tetrahedron is given by

$$\mathbf{w}^{23}(M)=\frac{a^{23}}{\det}(\overrightarrow{OM^1}\times\overrightarrow{OM^4}+\overrightarrow{\mathrm{M^1M^4}}\times\overrightarrow{OM})$$
$$\det=(\overrightarrow{\mathrm{M^1M^2}},\overrightarrow{\mathrm{M^1M^3}},\overrightarrow{\mathrm{M^1M^4}})$$
$$=\overrightarrow{\mathrm{M^1M^2}}\cdot(\overrightarrow{\mathrm{M^1M^3}}\times\overrightarrow{\mathrm{M^1M^4}})$$
$$a_{23}=\|\overrightarrow{\mathrm{M^2M^3}}\|.$$

The basis function can also be written using the barycentric coordinates of M $(\lambda_1,\lambda_2,\lambda_3,\lambda_4)$ and their gradients

$$\mathbf{w}^{23}=a^{23}(\lambda_2\nabla\lambda_3-\lambda_3\nabla\lambda_2)$$
$$\nabla\lambda_2=\frac{1}{\det}(\overrightarrow{\mathrm{M^1M^3}}\times\overrightarrow{\mathrm{M^1M^4}})$$
$$\nabla\lambda_3=\frac{1}{\det}(\overrightarrow{\mathrm{M^1M^4}}\times\overrightarrow{\mathrm{M^1M^2}}).$$

We then compute the cross product of the normal to triangle (M^1, M^2, M^3) with the basis function, and obtain

$$\mathbf{w}^{23}\times\hat{n}=\frac{a^{23}}{\det}(\lambda_2(\overrightarrow{\mathrm{M^1M^4}}\times\overrightarrow{\mathrm{M^1M^2}})\times\hat{n}$$
$$-\lambda_3(\overrightarrow{\mathrm{M^1M^3}}\times\overrightarrow{\mathrm{M^1M^4}})\times\hat{n}).$$

By using the double cross product formula and using $\overrightarrow{\mathrm{M^1M^2}}\cdot\hat{n}=\overrightarrow{\mathrm{M^1M^3}}\cdot\hat{n}=0$ we obtain

$$\mathbf{w}^{23}\times\hat{n}=\frac{a^{23}}{\det}(\lambda_2\overrightarrow{\mathrm{M^1M^2}}(\overrightarrow{\mathrm{M^1M^4}}\cdot\hat{n})$$
$$+\lambda_3\overrightarrow{\mathrm{M^1M^3}}(\overrightarrow{\mathrm{M^1M^4}}\cdot\hat{n})).$$

The quantity $\det\,(=(\overrightarrow{\mathrm{M^1M^2}},\overrightarrow{\mathrm{M^1M^3}},\overrightarrow{\mathrm{M^1M^4}}))$ can be rewritten using the surface T of the triangle (M^1,M^2,M^3)

$$(\overrightarrow{\mathrm{M^1M^2}},\overrightarrow{\mathrm{M^1M^3}},\overrightarrow{\mathrm{M^1M^4}})=(\overrightarrow{\mathrm{M^1M^2}}\times\overrightarrow{\mathrm{M^1M^3}})\cdot\overrightarrow{\mathrm{M^1M^4}}$$
$$=(2T\hat{n})\cdot\overrightarrow{\mathrm{M^2M^4}}$$
$$=2T(\hat{n}\cdot\overrightarrow{\mathrm{M^1M^4}}).$$

Finally, we obtain

$$\mathbf{w}^{23} \times \hat{n} = \frac{a^{23}}{2T}(\lambda_2 \overrightarrow{\mathrm{M}^1\mathrm{M}^2} + \lambda_3 \overrightarrow{\mathrm{M}^1\mathrm{M}^3}).$$

If M belongs to the triangle (M^1, M^2, M^3), its barycentric coordinates are $(\lambda_1, \lambda_2, \lambda_3, 0)$, and $\lambda_2 \overrightarrow{\mathrm{M}^1\mathrm{M}^2} + \lambda_3 \overrightarrow{\mathrm{M}^1\mathrm{M}^3} = \overrightarrow{\mathrm{M}^1\mathrm{M}}$. We recognize the Rao–Wilton–Glisson basis function associated to edge a^{23} (here the M^2M^3 edge has positive orientation for the Rao–Wilton–Glisson basis function).

This shows that a linear combination of volume edge elements

$$\mathbf{E} = \sum e_i \mathbf{w}_i$$

has the following trace on the boundary:

$$\mathbf{E} \times \hat{n} = \sum e_i (\mathbf{w}_i \times \hat{n}) = \sum e_i \mathbf{f}_i.$$

The trace $\mathbf{E} \times \hat{n}$ is a linear combination of Rao–Wilton–Glisson basis functions.

The surface unknown associated to edge a^{32} is the flux

$$\frac{1}{a^{32}} \int_{a^{32}} (\mathbf{E} \times \hat{n}) \cdot (\overrightarrow{\mathrm{M}^2\mathrm{M}^3} \times \hat{n})\, dl = \frac{1}{a^{32}} \int_{a^{32}} \mathbf{E} \cdot \overrightarrow{\mathrm{M}^2\mathrm{M}^3}\, dl$$

which is the circulation of $\mathbf{E}$ along edge a^{32}, i.e., the volume unknown corresponding to edge a^{32}.

In conclusion, the e_i unknowns on the boundary of the scatterer are shared by the volume edge element expansion and the surface edge element expansion.

APPENDIX B

The operator P is invertible when discretized with piecewise constant elements (P0) or with linear nodal elements (P1). But P is not invertible when discretized with H(div) or H(curl) edge elements. This difficulty stems from the fact that the $\hat{n} \times$ operator transforms vectors of H(div, Σ) into vectors of H(curl, Σ).

The elementary matrix for P for a triangle can be computed explicitly and is given by

$$P_T = -\frac{jk}{12} \begin{pmatrix} 0 & -a_1 a_2 & a_1 a_3 \\ a_1 a_2 & 0 & -a_2 a_3 \\ -a_1 a_3 & a_2 a_3 & 0 \end{pmatrix}.$$

a_1, a_2, a_3 being the lengths of the three edges of the triangle. This matrix has zero determinant and its columns C_i are related by $\Sigma_{i=1}^3 \frac{1}{a_i} C_i = 0$. Clearly, this relation between the columns still holds when a matrix P is assembled over a set of triangles.

An element of the elementary matrix of Q discretized with H(div) elements relating two triangles T and T' reads

$$Q_{ii'}(T, T') = -\frac{jk}{4\pi} \frac{a_i a_{i'}}{4TT'} \int_{T'} \int_{T} (\nabla' G) \cdot (\overrightarrow{\mathrm{M}^i\mathrm{M}} \times \overrightarrow{\mathrm{M}^{i'}\mathrm{M}'})\, ds\, ds'.$$

If the integral on M is evaluated at the centroid we see that the columns of the elementary matrix are related by

$$\Sigma_{i=1}^3 \frac{1}{a_i} Q_{ii'}(T, T') = -\frac{jk}{4\pi} \frac{a_{i'}}{4T'} \int_{T'} (\nabla' G) \cdot \left(\left(\Sigma_{i=1}^3 \overrightarrow{\mathrm{M}^i\mathrm{G}} \right) \times \overrightarrow{\mathrm{M}'^{i}\mathrm{M}'} \right) ds' = 0.$$

since $\Sigma_{i=1}^3 \overrightarrow{\mathrm{M}^i\mathrm{G}} = 0$. The columns of Q are related by the same relation as the columns of P. It follows that the operators P, Q and $P+Q$ discretized with H(div) elements are not invertible.

REFERENCES

[1] J. C. Nédélec, "Mixed finite elements in $\mathbb{R}^3$," *Numer. Math.*, vol. 35, pp. 315–341, 1980.

[2] A. Bossavit and J. C. Vérité, "A mixed FEM-BIEM method to solve 3-D Eddy-current problems," *IEEE Trans. Magn.*, vol. 18, pp. 431–435, Mar. 1982.

[3] M. L. Barton and Z. J. Cendes, "New vector finite elements for three-dimensional magnetic field computation," *J. Appl. Phys.*, vol. 61, pp. 3919–3921, Apr. 1987.

[4] A. Bossavit, "A rationale for edge elements in 3-D fields computations," *IEEE Trans. Magn.*, vol. 24, pp. 74–79, Jan. 1988.

[5] R. D. Graglia, D. R. Wilton, and A. F. Peterson, "Higher order interpolatory vector bases for computational electromagnetics," *IEEE Trans. Antennas Propagat.*, vol. 45, pp. 329–342, Mar. 1997.

[6] P. A. Raviart and J. M. Thomas, "A mixed finite element method for second-order elliptic problems," *Lecture Notes in Maths. N606*, Springer Verlag, Berlin, 1977.

[7] S. M. Rao, D. R. Wilton, and A. W. Glisson, "Electromagnetic scattering by surfaces of any shape," *IEEE Trans. Antennas Propagat.*, vol. AP-30, pp. 409–418, May 1982.

[8] D. R. Wilton, "Review of current status and trends in the use of integral equations in computational electromagnetics," *Electromagnetics*, vol. 12, pp. 287–341, 1992.

[9] L. N. Medgyesi-mitschang, J. M. Putnam, and M. B. Gedera, "Generalized method of moments for three-dimensional penetrable scatterers," *J. Opt. Soc. Amer. A*, vol. 11, no. 4, pp. 1383–1398, Apr. 1994.

[10] K. D. Paulsen, D. R. Lynch, and J. W. Strohbehn, "Three-dimensional finite, boundary, and hybrid element solutions of the Maxwell equations for lossy dielectric media," *IEEE Trans. Microwave Theory Tech.*, vol. 36, pp. 682–693, Apr. 1988.

[11] J.-M. Jin and J. L. Volakis, "A finite element-boundary integral formulation for scattering by three-dimensional cavity-backed apertures," *IEEE Trans. Antennas Propagat.*, vol. 39, pp. 97–104, Jan. 1991.

[12] J. J. Angélini, C. Soize, and P. Soudais, "Hybrid numerical method for harmonic 3-D Maxwell equations: Scattering by a mixed conducting and inhomogeneous anisotropic dielectric medium," *IEEE Trans. Antennas Propagat.*, vol. 41, pp. 66–76, Jan. 1993.

[13] P. Soudais, "Computation of the electromagnetic scattering from complex 3D objects by a hybrid FEM/BEM method," *J. Electromagn. Waves Applicat.*, vol. 9, pp. 871–886, July 1995.

[14] X. C. Yuan, "Three-dimensional electromagnetic scattering from inhomogeneous objects by the hybrid moment and finite element method," *IEEE Trans. Microwave Theory Tech.*, vol. 38, pp. 1053–1058, Aug. 1990.

[15] J.-M. Jin and J. L. Volakis, "Electromagnetic scattering by and transmission through a three-dimensional slot in a thick conducting plane," *IEEE Trans. Antennas Propagat.*, vol. 39, pp. 543–550, Apr. 1991.

[16] V. Levillain, "Couplage éléments finis-équations intégrales pour la résolution des équations de Maxwell en milieux hétérogènes," Ph.D. dissertation, École Polytechnique, 1991.

[17] X.-Q. Sheng, J.-M. Jin, J. Song, C.-C. Lu, and W. C. Chew, "On the formulation of hybrid finite-element and boundary-integral methods for 3-D scattering," *IEEE Trans. Antennas Propagat.*, vol. 46, pp. 303–311, Mar. 1998.

[18] P. Soudais, "Iterative solution of a 3-D scattering problem from arbitrary shaped multidielectric and multiconducting bodies," *IEEE Trans. Antennas Propagat.*, vol. 42, pp. 954–959, July 1994.

[19] A. F. Peterson, "Analysis of heterogeneous electromagnetic scatterers: Research progress the past decade," *Proc. IEEE*, vol. 79, pp. 1431–1441, Oct. 1991.

[20] J. M. Jin, *The Finite Element Method in Electromagnetics*. New York: Wiley, 1993.

[21] S. M. Rao, T. K. Sarkar, P. Midya, and A. R. Djordević, "Electromagnetic radiation and scattering from finite conducting and dielectric structures: Surface/surface formulations," *IEEE Trans. Antennas Propagat.*, vol. 39, pp. 1034–1037, July 1991.
[22] R. D. Graglia, P. L. E. Uslenghi, and R. S. Zich, "Moment method with isoparametric elements for three-dimensional anisotropic scatterers," *Proc. IEEE*, vol. 77, pp. 750–760, May 1989.

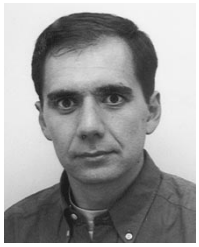

Paul Soudais (M'94) received the Diplôme d'Ingénieur degree in 1988 and the Ph.D. degree in 1995, both from the Ecole Centrale de Paris.

Since 1989, he has beeen working as a Researcher at O.N.E.R.A., first in the Structures Department and later in the Electromagnetism and Radar Department. In 1994 he participated in a U.S.–French Scientist and Engineer Exchange program as a visiting researcher at the Department of Electrical Engineering and Computer Science at the University of Illinois at Chicago.

Hervé Stève received the M.S. degree in 1986 from the University of Nice and the Ph.D. degree in 1988 from INRIA Sophia-Antipolis, both in applied mathematics.

Since 1989, he has been working as a Research Engineer at Dassault Aviation first in the Numerical Analysis group, and then in the Electromagnetism group.

Fabrice Dubois, photograph and biography not available at the time of publication.